Interaction of Water, Alkyl Hydroperoxide, and Allylic Alcohol with a Single-Site Homogeneous Ti−Si Epoxidation Catalyst: A Spectroscopic and Computational Study†

Atsushi Urakawa, Thomas Bürgi,‡ Peter Skrabal, Felix Bangerter, and Alfons Baiker*

Department of Chemistry and Applied Biosciences, Swiss Federal Institute of Technology, ETH-Hönggerberg, CH-8093 Zürich, Switzerland

Received: March 5, 2004; In Final Form: May 21, 2004

Tetrakis(trimethylsiloxy)titanium (TTMST, $Ti(OSiMe_3)_4$) possesses an isolated Ti center and is a highly active homogeneous catalyst in epoxidation of various olefins. The structure of TTMST resembles that of the active sites in some heterogeneous Ti−Si epoxidation catalysts, especially silylated titania−silica mixed oxides. Water cleaves the Ti−O−Si bond and deactivates the catalyst. An alkyl hydroperoxide, TBHP (*tert*-butyl hydroperoxide), does not cleave the Ti−O−Si bond, but interacts via weak hydrogen-bonding as supported by NMR, DOSY, IR, and computational studies. ATR−IR spectroscopy combined with computational investigations shows that more than one, that is, up to four, TBHP can undergo hydrogen-bonding with TTMST, leading to the activation of the O−O bond of TBHP. The greater the number of TBHP molecules that form hydrogen bonds to TTMST, the more electrophilic the O−O bond becomes, and the more active the complex is for epoxidation. An allylic alcohol, 2-cyclohexen-1-ol, does not interact strongly with TTMST, but the interaction is prominent when it interacts with the TTMST−TBHP complex. On the basis of the experimental and theoretical findings, a hydrogen-bond-assisted epoxidation mechanism of TTMST is suggested.

Introduction

Titanium-containing homogeneous and heterogeneous catalysts are known to be active in various selective oxidation reactions, especially in stereo- and regioselective epoxidation.[1,2] Sharpless asymmetric epoxidation catalyst is the most prominent example among homogeneous catalysts,[3−6] while TS-1 (titania−silicate-1) is best known in heterogeneous catalysis.[7,8] A number of experimental and theoretical studies dealing with TS-1 suggest possible reaction mechanisms.[9−17] Model clusters or embedded systems describing the active center have been applied to investigate the epoxidation mechanism, but the complexity of heterogeneous Ti−Si catalysts makes the modeling difficult, and consequently, the nature of the active site and the relevance of cluster model calculations are still debated. Various titanium silsesquioxanes as a soluble model of active TS-1 sites have been reported often using TBHP (*tert*-butyl hydroperoxide) as oxidant.[18−22] The main difference between TS-1 and the model titanium silsesquioxanes is that the latter are inactive with aqueous hydrogen peroxide, except for grafted titanium polysiloxanes.[23] Considerable efforts have been made to enhance the applicability of heterogeneous catalysts in epoxidation, and besides TS-1, a wide variety of titania−silica mixed oxides have been reported.[24−27] Among titania−silica mixed oxides, aerogels are excellent catalysts because of the high surface area and relatively large pore size, which affords epoxidation of larger and more complex molecules than simple linear molecules. Despite their excellent catalytic performance, the amorphous nature in addition to the inherent complexity of the mixed oxides results in various active sites and retards detailed investigation of the reaction mechanism.[28]

Recently, tetrakis(trimethylsiloxy)titanium (TTMST, $Ti(OSiMe_3)_4$) was suggested to be a good soluble homogeneous model catalyst mimicking the highly active isolated tetrahedral Ti sites in silylated titania−silica mixed oxides.[29] Although a similar catalyst, $Ti(OSiPh_3)_4$, is inactive in epoxidation,[30] TTMST shows excellent catalytic properties with various olefins and especially gives 100% regio- and stereoselectivity for geraniol and 2-cyclohexen-1-ol (CHol, cyclohexenol) using TBHP as oxidant in an apolar solvent. Addition of water to the TTMST catalytic system has negative effects on the epoxidation activity and selectivity as similarly reported for titania−silica mixed oxides. Elucidating how TBHP and CHol interact with TTMST is crucial for understanding the epoxidation mechanism. TTMST not only possesses excellent catalytic properties, but also has the inherent advantage of homogeneous catalysts in that full modeling of the catalytic system is feasible with less assumptions and simplifications.

In this work, the molecular interactions of water, TBHP, and CHol with TTMST were studied using NMR and IR spectroscopy. Computational methods were applied to understand the interactions and the activation mechanism during epoxidation, especially the activation of the O−O bond of TBHP. The possible differences in the epoxidation mechanism between TS-1−H_2O_2 and TTMST−TBHP as catalyst−oxidant pairs and also the effect of water on the active site are discussed.

Experimental Section

Materials. TTMST ($Ti(OSiMe_3)_4$; ABCR, 99.5%) and CHol (2-cyclohexen-1-ol; Fluka, 99.7%) were used as received. Toluene (Fluka, 99.5%) and TBHP (*tert*-butyl hydroperoxide; Fluka, 5.5 N in nonane) were stored over molecular sieves 4 Å.

Spectroscopic Methods. ATR-IR spectroscopy was applied to record full-range spectra by minimizing the large absorption

† Part of the special issue "Michel Boudart Festschrift".

* To whom correspondence should be addressed. Phone: +41 1 632 31 53. Fax: +41 1 632 11 63. E-mail: baiker@chem.ethz.ch.

‡ Current address: Department of Chemistry, University of Neuchâtel, Neuchâtel, Switzerland.

10.1021/jp048999q CCC: $30.25 © 2005 American Chemical Society
Published on Web 07/07/2004

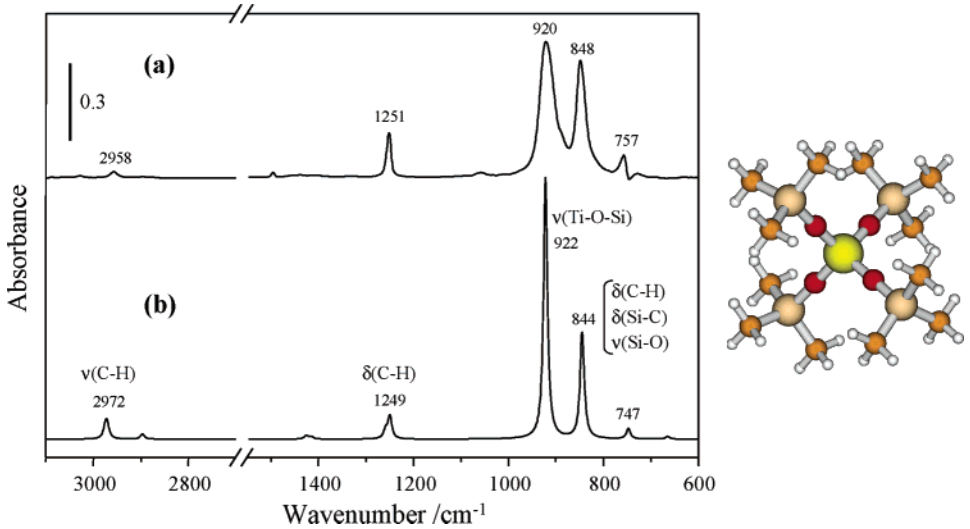

Figure 1. Comparisons between experimental and calculated IR spectra: (a) 0.05 M TTMST in toluene at 300 K; (b) the calculated spectrum (scaled by 0.955).

by abundant solvent molecules in solution. In addition, the used ATR-IR cell, which has an inlet and an outlet, allows fast exchange of the sample solution, which is advantageous when the evolution of interaction and reaction is studied. The spectra were recorded on a Bruker IFS-66 spectrometer equipped with a liquid nitrogen cooled MCT detector using an ATR-IR attachment (Optispec). A ZnSe crystal was used for the internal reflection element. The angle of incidence and the number of active reflections were close to 45° and 8, respectively. Spectra were obtained by accumulating 200 scans at 1 cm^{-1} resolution.

^1H (500.133 MHz), ^{13}C (125.773 MHz), and ^{29}Si (99.355 MHz) NMR spectra were recorded on a Bruker AVANCE 500 spectrometer (11.7467 T) equipped with a 5 mm broad-band probe with an actively shielded *z*-gradient coil and a pulsed gradient unit for magnetic field pulse gradients of 56 G cm^{-1}. Toluene-d_8 (99.8%) was used as a solvent, and the chemical shifts are referenced to the peak for internal TMS. The gradient strength was calibrated with the diffusion coefficient of HDO in D_2O at 298 K.[31] The diffusion coefficients of the species discussed in this work were obtained from DOSY (diffusion-ordered spectroscopy) experiments using stimulated echoes with a bipolar gradient pulse pair and one spoil gradient pulse (2D pulse program stebpgp1s, Bruker pulse programs for XWinNMR 3.1/3.5). After Fourier transformation and baseline correction in F2, data processing by the SimFit algorithm in XWinNMR 3.5 was done. Typically, a gradient ramp file was used to produce gradient amplitudes scaled to rectangular gradients, linearly spaced in 16 steps between 0.721 and 34.227 G cm^{-1}. The duration of the magnetic field pulse gradient (δ) was between 2 and 4 ms, and the diffusion time (Δ) was between 100 and 400 ms. The temperature was controlled with a nitrogen flow of 400 L h^{-1} to avoid temperature fluctuations of more than 0.1 deg. In each PFG (pulsed field gradient) experiment a series of 8−16 spectra were collected with an FID resolution of 0.8 Hz.

Computational Methods. Quantum chemical calculations were performed using Gaussian 98 and 03.[32,33] A density functional hybrid method with Becke's three-parameter functional and the nonlocal correction of Perdew and Wang (B3PW91)[34,35] was applied to calculate harmonic vibrational frequencies after complete geometry optimization. A 6-311G-(d) basis set was applied for all the atoms except Ti. For Ti, a basis set of (14s9p5d)/[9s5p3d] with an additional f polarization function was used.[36−38] BSSE (basis set superposition error) was corrected using counterpoise approximation[39] for the calculation of interaction energies. All calculations were carried out considering an isolated gas-phase molecule or complex without solvent effects. IR spectra are shown as the sum of Lorentzian lines taking the calculated IR intensity of a normal mode as the height at each frequency.

Results and Discussion

Equilibrium Geometry. Experimental and calculated IR spectra and an optimized geometry of TTMST are shown in Figure 1. The angle of the Ti−O−Si bond was close to 180°. The bond lengths and angles and the Mulliken atomic charges are shown in Table 2. The asymmetric Ti−O−Si stretching vibrations at 920 cm^{-1} are nearly triply degenerate, and they represent the main characteristic vibrational mode of this molecule. The calculated vibrational spectrum of TTMST well-reproduced the experimental spectrum and allowed the vibrational modes to be assigned. This good agreement ensures the accuracy of the used method and indicates little TTMST−solvent interaction.

Experimental and theoretical vibrational spectra of TBHP and CHol are also in good agreement, and the most probable conformation of CHol in toluene was determined on the basis of the vibrational spectra and electronic energies (details are described in the Supporting Information, Figures 1(S) and 2(S)).

Interaction of Water with TTMST. Water was added to 0.005 M TTMST solution in toluene-d_8 (TTMST:H_2O = 1:10), and the interaction and reaction were followed by ^1H and ^{29}Si NMR (Figure 2). Clearly, Me_3SiOH was formed by the hydrolysis of TTMST. After a period of time (ca. 24 h in an NMR tube), a white precipitate was observed. This is clear evidence of the Ti−O−Si bond cleavage by hydrolysis. IR experiments also showed a decrease in ν(Ti−O−Si) at 920 cm^{-1}, which supports the Ti−O−Si bond breaking (not shown here).

Interaction of TBHP with TTMST. The TBHP concentration with respect to TTMST was varied (TTMST:TBHP = 1:0−10) at 243 K. In ^{29}Si NMR, it was practically not possible to measure spectra above 243 K. The peaks became too broad, and the spectra were too noisy. This is indicative of a relatively slow interaction equilibrium of TBHP with TTMST. In the case of the previous water−TTMST interaction experiment, clear sharp peaks were observed in ^{29}Si NMR spectra even at 300 K.

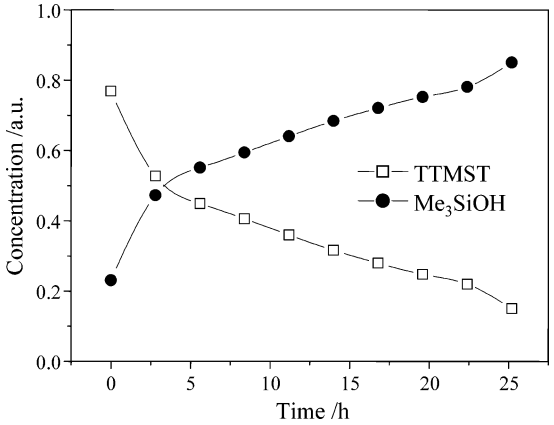

Figure 2. Evolution of the ^{1}H NMR peak area for TTMST (δ = 0.222−0.223 ppm) and Me_3SiOH (δ = 0.035−0.039 ppm; Me_3SiOH formation was confirmed by δ = 14.9 ppm in ^{29}Si NMR), 0.005 M TTMST in toluene-d_8, TTMST:H_2O = 1:10, at 300 K in an NMR tube (no mixing).

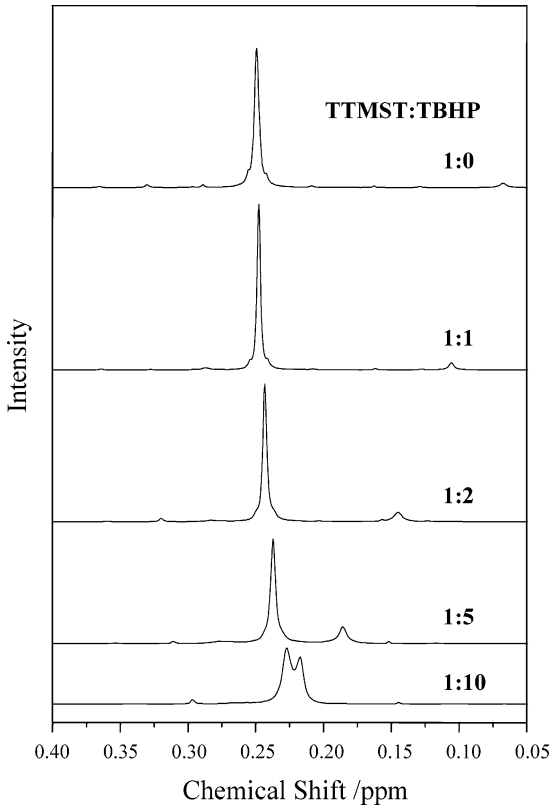

Figure 3. ^{1}H NMR spectra of TTMST−TBHP solution of different TBHP concentrations at 243 K, 0.05 M TTMST in toluene-d_8.

The ^{29}Si NMR spectra of TTMST−TBHP solution at 243 K will be shown later in comparison with those of TTMST−CHol solution and also solutions under reaction conditions (TTMST−TBHP−CHol).

In ^{1}H NMR, broader peaks of TTMST (0.23−0.25 ppm) were observed at a higher concentration of TBHP (Figure 3). A peak near the catalyst peak appeared (0.1−0.22 ppm), and its intensity increased and it was shifted to lower field as the TBHP concentration was raised. Also, the effect of temperature on the ^{1}H NMR chemical shift of TTMST was examined. Interestingly, in addition to the broadening of the peaks at higher temperatures, the additional peak due to TBHP addition shifted more significantly with temperature to higher field than the original TTMST peak (Figure 4). The integral comprising the TTMST and the additional peak was constant at different conditions

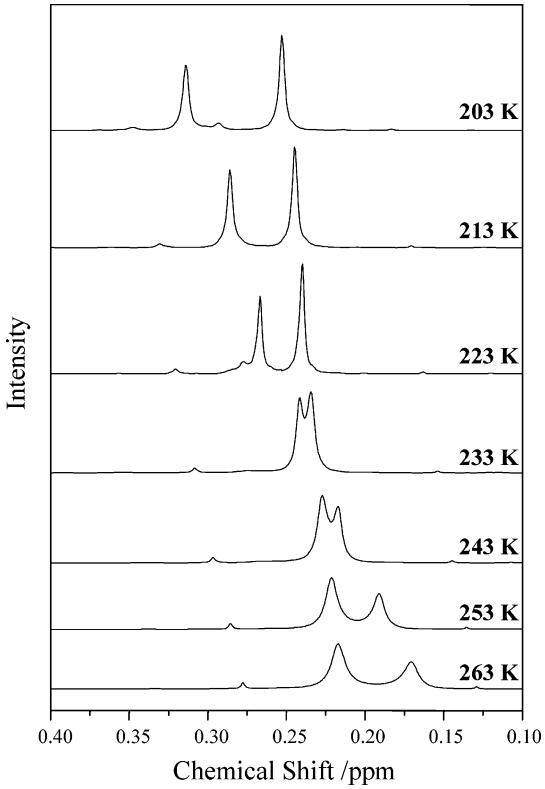

Figure 4. ^{1}H NMR spectra of TTMST−TBHP solution (TTMST:TBHP = 1:10) at different temperatures, 0.05 M TTMST in toluene-d_8.

(different temperatures and TBHP concentrations). This indicated that the compound or complex corresponding to the additional peak originates from TTMST, or that the two peaks are due to the same TTMST complex with different magnetic sites of the methyl groups. Neither cleavage of the Ti−O−Si bond nor Me_3SiOH formation by TBHP within 24 h at 300 K, at which epoxidation reaction occurs in the presence of CHol, was confirmed by ^{1}H and ^{29}Si NMR.

To investigate possible species responsible for the peak appearing upon TBHP addition, diffusivity of the molecule or complex corresponding to the peak was studied by ^{1}H DOSY. The radii of molecules or complexes were estimated using the Stokes−Einstein equation[40] $D = kT/(6\pi\eta r)$ (where k is the Boltzmann constant, η is the viscosity of the medium, and r is the diameter of the particle), which is derived for a macroscopic spherical particle drifting in a viscous continuous medium. The diffusion coefficients and the estimated radii are shown in Table 1. The diffusion coefficients of TBHP were calculated on the basis of the OOH proton due to the peak overlap of the TBHP methyl proton with nonane protons (TBHP solution in nonane was used throughout). Although the Stokes−Einstein equation assumes a sphere as the molecular shape and does not take the molecular interactions into account, the radius of TTMST at low temperatures, at 213 and 223 K, was well estimated (the distance between the center Ti atom and the farthest methyl hydrogen from the optimized geometry was 5.47 Å). The overestimation of the radius of TBHP by itself in toluene indicates the intermolecular interaction by hydrogen bonds. The two peaks originating from TTMST showed different diffusion behaviors, which proves that they are from different species; that is, the two ^{1}H NMR peaks do not originate from protons in the same molecule or complex. The radius of TTMST(2) was larger than that of TTMST(1) at all temperatures.

In IR, dramatic changes in the Ti−O−Si stretching modes

TABLE 1: Diffusion Coefficients ($\times 10^{-10}$ m^2/s) and Estimated Radii (Å) at Different Temperatures Measured by DOSY[a]

	TTMST		TBHP		TTMST + TBHP			
temp (K)	toluene	TTMST	toluene	TBHP	toluene	TBHP	TTMST(1)	TTMST(2)
				Diffusion Coeffici ents ($\times 10^{-10}$ m^2/s)				
213	2.07	0.96	2.18	1.05	2.17	1.01	1.02	0.86
223	3.23	1.46	3.69	1.72	4.04	1.62	1.49	1.37
298	20.4	10.8	20.4	[b]	20.4	18.2	14.1	12.9
				Estimated Radii (Å)				
213	2.71	5.85	2.57	5.35	2.59	5.56	5.50	6.53
223	2.44	5.40	2.14	4.58	1.95	4.87	5.29	5.76
298	1.94	3.67	1.94	[b]	1.94	2.18	2.81	3.07

[a] TTMST(1) is the less mobile peak and TTMST(2) is the more mobile peak in ^{1}H NMR upon temperature variations (Figure 4). To calculate the radii, the viscosity of toluene was estimated using the data in the literature[49] and fitting with 6th degree polynomial expansion. [b] The signal was too broad to be observed.

TABLE 2: Bond Lengths, Angles, and Mulliken Atomic Charges of the Molecules and the Complexes[a]

Bond Lengths and Angles

	TTMST	TBHP	TTMST + TBHP	TTMST + 2TBHP	TTMST + 3TBHP	TTMST + 4TBHP	TTMSS	TTMSS + TBHP
Ti−O	1.793		1.787	1.781	1.771			
Ti−O (H-bonded)			1.828	1.820	1.814	1.806		
Si−O (Si(center))							1.621	1.621
Si−O (H-bonded)								1.650
O−Si	1.663		1.670	1.675	1.684		1.651	1.663
O−Si (H-bonded)			1.681	1.687	1.692	1.698		1.687
(OO)H···O (<M, Si)			1.912	1.933	1.944	1.967		1.901
O−O (TBHP)		1.438	1.448	1.445	1.446	1.445		1.449
O−H (TBHP)		0.966	0.976	0.975	0.975			0.976
∠(M−O−Si)	179.66		**149.47**	**147.92**	**147.53**	**148.23**	179.78	**142.84**
	179.89		165.52	**148.88**	**149.77**	**148.87**	179.90	149.42
	179.94		172.58	166.64	**150.85**	**149.29**	179.94	161.17
	179.98		172.91	167.04	165.41	**150.17**	179.97	171.16

Mulliken Charges

TTMST		TTMSS		TBHP		CHol	
Ti	1.80	Si(center)	1.54	O(−H)	−0.42	O	−0.56
Si	1.38	Si	1.43	O(−tBu)	−0.23	H(−O)	0.38
O	−0.83	O	−0.79	H(−OO)	0.41		

[a] The bond lengths and atomic charges are averaged when more than one bond or atom was involved in a similar environment. Bond lengths and angles are shown in angstroms and degrees, respectively. M represents Ti for TTMST and Si for TTMSS. The angle values are given in bold when the M−O−Si bond is hydrogen-bonded by TBHP.

were observed upon TBHP addition (Figure 5). A band around 890 cm^{-1} appeared as the absorbance of the Ti−O−Si stretching vibrational frequencies around 920 cm^{-1} decreased. The relative absorbance of the bands at 890 and 920 cm^{-1} changed as the concentration of TBHP was varied (Figure 5). The analysis of the OH stretching region (3000−3700 cm^{-1}) showed hydrogen-bonding within TBHP and between TBHP and TTMST. In the presence of TTMST in solution the ratio of free or very weakly interacting TBHP increases with respect to TBHP interacting with itself (the details are available in the Supporting Information, Figure 3(S)).

TiOOH(η^1) or TiOOH(η^2) complexes with one or two oxygen atoms of TBHP coordinating to the Ti center are possible species formed upon addition of TBHP to TTMST. However, the formation as such of complexes does not explain the ^{1}H chemical shift changes induced by temperature and concentration variations. The temperature and concentration dependence of the chemical shifts implies a flexible and dynamic structure. Theoretical investigations of TiOOH(η^1) and TiOOH(η^2) complexes resulted in no energetic minimum (B3PW91/3-21G, within ground-state assumption); instead TBHP hydrogen-bonded to TTMST was found as a minimum. First, interaction of TTMST with one TBHP molecule was investigated. Several relatively stable conformations could exist for a TTMST−TBHP hydrogen-bonding complex with a static model investigation. Various starting geometries converged into mainly three structures at the B3PW91/3-21G level of theory with very similar energy. A structure among the three with the lowest energy was assumed as the global minimum structure, and further the structure was optimized and the harmonic frequencies and normal modes were analyzed using the method described in the Experimental Section. The binding energy of the hydrogen-bonding was estimated to be only 1.27 kJ/mol at the same level of theory after BSSE was taken into account. Although this interaction energy is small, the effect of the hydrogen-bonding on the calculated spectrum is significant. Figure 6 shows the calculated IR spectrum of TTMST with one hydrogen-bonded TBHP molecule. Upon hydrogen-bonding of TBHP, one mode of the three nearly degenerated Ti−O−Si vibrations is coupled with the O−H bending vibration and red-shifted from 920 to 875 cm^{-1}, which makes the IR intensity of the Ti−O−Si stretching at 920 cm^{-1} smaller. This is in good agreement with the experimental observations (Figure 5).

Furthermore, geometry optimization and harmonic frequency analysis were carried out for hydrogen-bonded complexes with two, three, and four TBHP molecules. One possible geometry for each complex was considered, and therefore, the complex geometries may not be at the global minimum of the potential energy surface. However, the series should show a tendency of IR spectral change when more TBHP molecules interact with TTMST. When two TBHP molecules are hydrogen-bonded, two of the three degenerate Ti−O−Si stretching vibrations red-shift

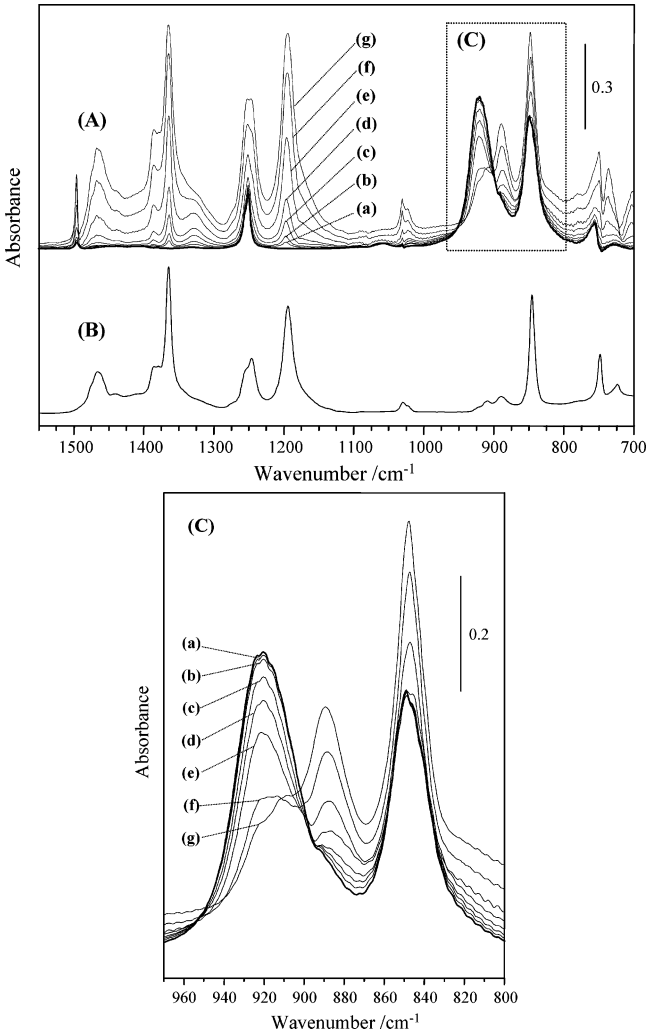

Figure 5. (A) ATR-IR spectra of TTMST−TBHP solution in toluene. The bold line represents TTMST in toluene. Traces a−g correspond to TTMST:TBHP = 1:1, 1:2, 1:5, 1:10, 1:30, 1:50, and 1:80, respectively (0.05 M TTMST in toluene at 300 K for all the solutions). (B) ATR-IR spectrum of 5.5 M TBHP in nonane at 300 K. (C) ATR-IR spectra of the ν(Ti−O−Si) region.

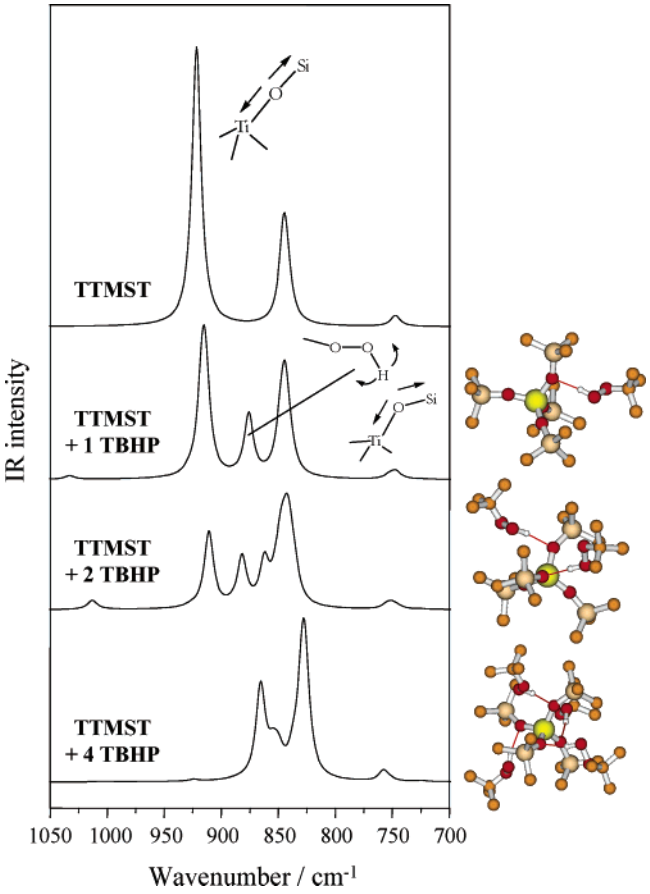

Figure 6. Calculated IR spectra of TTMST and TTMST complexes with one, two, and four hydrogen-bonding TBHP molecules (scaled by 0.955) and the optimized structures. For clarity hydrogens are not shown except hydrogens involved in hydrogen-bonding.

as shown in Figure 6. Moreover, the three Ti−O−Si vibrations are red-shifted to 865 cm^{-1} when all the Ti−O−Si bonds are hydrogen-bonded by four TBHP molecules. When TBHP forms the hydrogen-bonded complexes, the distance between the center Ti atom and the farthest methyl hydrogen of TBHP is approximately 7.5 Å, which is larger than the radius estimated from DOSY, but the radii of the latter may be significantly underestimated due to the spherical shape assumption of the complex. Comparing the IR spectra (Figure 5) with the theoretical IR spectra (Figure 6) indicates that not all the Ti−O−Si bonds are hydrogen-bonded with TBHP under the conditions of the current study. It should be noted that in ^{1}H NMR only one additional peak, most likely of the TTMST−TBHP complex, was observed. This is another indication of high mobility of TBHP around TTMST, and therefore, the peak represents an average on the time scale of the NMR measurements. The experimental and theoretical investigations support hydrogen-bonding as the main interaction between TTMST and TBHP. The effect of the hydrogen-bonding on the activation of the O−O bond in TBHP during epoxidation will be discussed later.

Interaction of CHol with TTMST. Interaction of CHol with TTMST was also examined by IR, NMR, and computational

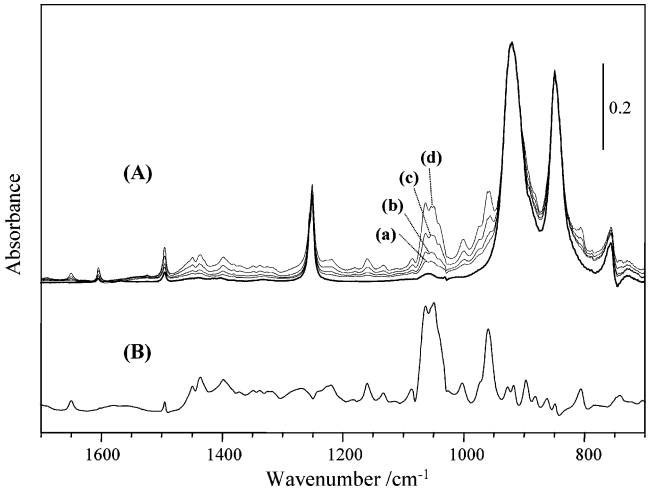

Figure 7. (A) ATR-IR spectra of a TTMST and CHol mixture in toluene. The bold line represents TTMST in toluene. Traces a−d correspond to TTMST:CHol = 1:1, 1:2, 1:5, and 1:10, respectively (0.05 M TTMST for all the solutions, at 300 K). (B) ATR-IR spectrum of 0.5 M CHol in toluene at 300 K.

means. Contrary to the TTMST−TBHP mixture, there was no significant change in the Ti−O−Si vibration upon the addition of CHol (Figure 7). Also, in ^{1}H and ^{29}Si NMR no remarkable change was observed (the details are discussed in the next section in comparison with the reaction mixture). This weak interaction of CHol with TTMST was also supported by theoretical calculations (details are described in the Supporting Information, Figure 4(S)). Thus, we suggest that CHol itself

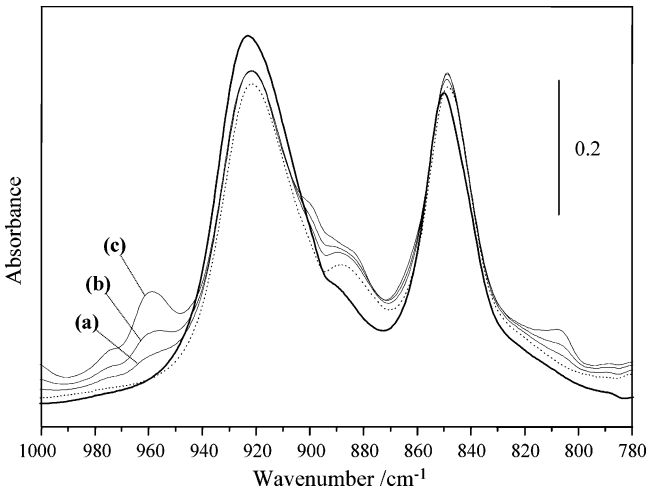

Figure 8. ATR-IR spectra of a TTMST, TBHP, and CHol mixture in toluene. The bold line represents TTMST in toluene. The dotted line represents the TTMST:TBHP = 1:10 solution in toluene. Traces a−c correspond to TTMST:TBHP:CHol = 1:10:2, 1:10:5, and 1:10:10, respectively (0.05 M TTMST for all the solutions, at 300 K).

does not interact strongly with TTMST. In particular, it does not form hydrogen bonds.

Interaction of TBHP and CHol with TTMST. The state of TTMST in the presence of both TBHP and CHol, i.e., under epoxidation conditions, was examined by IR. The ratio of the TTMST:TBHP = 1:10 solution was kept constant, while the concentration of CHol was varied. Note that TBHP addition to TTMST dissolved in toluene resulted in a decrease of the intensity of the Ti−O−Si band. Upon CHol addition, the decreased Ti−O−Si band slightly regained its intensity (Figure 8). The different CHol concentrations did not affect the degree of this intensity increase.

One possible explanation for this observation is the elimination of TBHP from the TTMST matrix (the space in the proximity of TTMST) by competing CHol. This is, however, unlikely due to the very weak interaction of CHol with TTMST. Another possibility is that CHol interacts with TBHP in the TTMST matrix. Since the interaction between TTMST and TBHP is decreased by the interaction of TBHP−CHol, the intensity of the Ti−O−Si stretching vibration could be regained. Also, the constant intensity increase of the latter at the different CHol concentrations implies that CHol interacts with TTMST−TBHP complexes with a certain ratio, e.g., 1:1, TBHP to CHol.

The interaction among TTMST, TBHP, and CHol was studied by ^{1}H, ^{13}C, and ^{29}Si NMR. A solution containing the compounds in the ratio TTMST:TBHP:CHol = 1:10:10 (TBHP and/or CHol are absent for TTMST, TTMST−TBHP, and TTMST−CHol) was chosen. The ^{13}C NMR measurements showed exactly the same trends as the ^{29}Si NMR investigations; therefore, the ^{13}C NMR results are not shown here. When CHol was added to TTMST, a small peak appeared (Figure 9). In contrast, the change in the spectrum was very significant when TBHP was added to the TTMST solution in both ^{1}H and ^{29}Si NMR. In ^{1}H, ^{13}C, and ^{29}Si NMR, the TTMST−TBHP solution showed almost the same intensity for both peaks. Note that the peak which appeared upon TBHP addition was very mobile regarding the ^{1}H NMR chemical shift at different TBHP concentrations and temperatures as shown in Figures 3 and 4. However, the similar peaks in ^{1}H NMR do not mean that the protons are in similar environments. When CHol was added to TTMST−TBHP solution, the chemical shift difference between TTMST and the additional peak became smaller in ^{29}Si and ^{13}C NMR, whereas an opposite trend was observed in ^{1}H NMR. The effect of CHol addition to TTMST−TBHP solution was prominent in comparison with that of the addition of CHol to TTMST solution, which indicates that the interaction of CHol with the TTMST matrix is remarkably enhanced when TTMST interacts with TBHP.

The changes in the ^{29}Si NMR chemical shift of the reaction mixture before and after the reaction were investigated (Figure 9) at two reaction conditions, namely (a) 20 h at 300 K and (b) 15.5 h at 333 K (in an NMR tube, no mixing). The conversions of CHol were (a) 31% and (b) 95%, respectively. When the reaction proceeded, the TTMST peak (∼13.6 ppm in ^{29}Si NMR, corresponding to ∼0.22 ppm in ^{1}H NMR judging from the peak area) decreased. Especially when the reaction was almost complete (condition b), the TTMST peak almost disappeared. On the contrary, the complex peak (∼15.3 ppm in ^{29}Si NMR, ∼0.26 ppm in ^{1}H NMR before the reaction) became sharper and gained intensity. The peak shifted upfield toward that of TTMST in ^{29}Si NMR and downfield in ^{1}H NMR. During the reactions, the sum of the two peak areas in ^{1}H NMR was constant, which confirms that during epoxidation no cleavage occurs. From a structural point of view, ^{1}H NMR should be more sensitive to the environment around the TTMST matrix, while ^{29}Si NMR should be more sensitive to the state and structure of TTMST. In ^{29}Si NMR, upon addition of CHol to TTMST−TBHP solution the complex peak shifted upfield toward the chemical shift of the uncomplexed TTMST observed upon addition of TBHP and CHol, and the TTMST peak (^{29}Si, ∼13.6 ppm) gradually decreased. This implies that the TTMST in the complex readjusted to the original TTMST state. In ^{1}H NMR, the additional peak moved away from the TTMST peak which also gradually decreased during the reaction. In both ^{1}H and ^{29}Si NMR, the line width of the peak became similar to that of the TTMST peak without reactants as the reaction proceeded. The result that the ^{1}H chemical shift does not move toward TTMST is reasonable considering that the environment near TTMST changes as the reaction proceeds due to the epoxide and *tert*-butyl alcohol formation. An interesting observation is that the TTMST in the complex seems to return to the original state, but the two peaks in NMR are distinct. On the NMR time scale, the uncomplexed TTMST apparently exists and decreases in time during epoxidation.

Activation toward Epoxidation and the Role of Ti. In the preceding section, mainly the interaction of TBHP and CHol with TTMST was considered, indicating that the TBHP hydrogen-bonded complexes may play a key role during epoxidation. It remains to be explored whether hydrogen-bonding is sufficient to activate the reaction.

Generally, it is agreed that epoxidation by peroxo species (peroxo, hydroperoxo complex, or peroxide) occurs via interaction between an occupied C=C π-bonding orbital, π(C=C) (often the HOMO of an olefin), and an unoccupied O−O σ-antibonding orbital, σ^*(O−O) (often an LUMO in the case of peroxide). The electrophilic character of σ^*(O−O) is often related to the reactivity.[41−44] Rösch and co-workers have theoretically analyzed the reactivity of various transition-metal peroxo complexes by σ^*(O−O) orbital energies in comparison with the activation energies.[42−44] In this section, the electrophilic character of the O−O bond is analyzed in a similar manner using Kohn−Sham orbitals and the corresponding energies.

Figure 10 shows the interactions between σ^*(O−O) of TBHP (LUMO) and the energetically closest orbital of TTMST (LUMO + 5). The σ^*(O−O) orbitals of the complexes are located at the LUMO + 5 and LUMO + (5 + n) (n is from 1

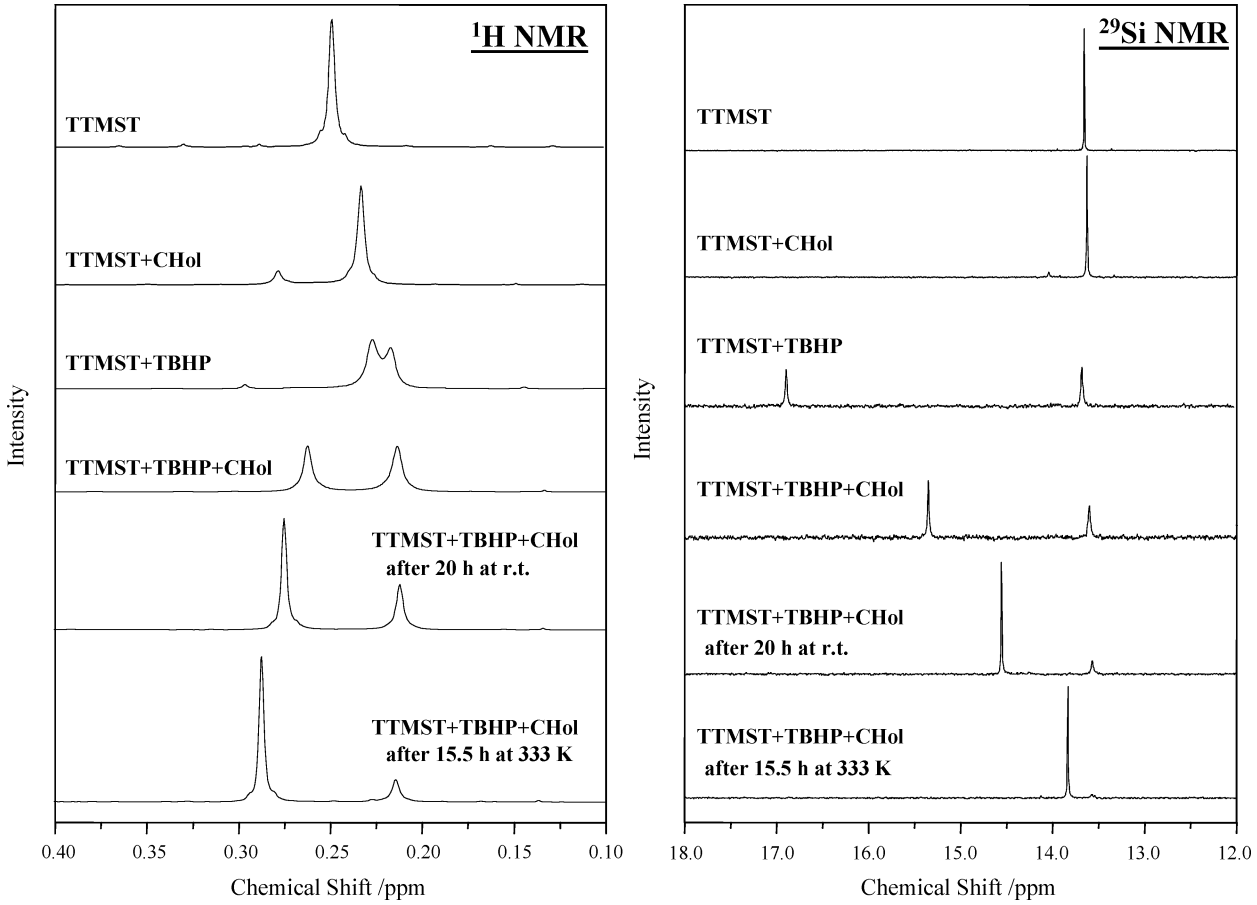

Figure 9. ^{1}H and ^{29}Si NMR spectra of various TTMST−TBHP−CHol mixtures (0.05 M TTMST in toluene-d_8, TTMST:TBHP:CHol = 1:10:10, where TBHP and/or CHol are absent for TTMST, TTMST + TBHP, and TTMST + CHol) at 243 K. The bottom two spectra are measured at 243 K after reactions of 20 h at room temperature and 15.5 h at 333 K (31% and 95% CHol conversion, respectively).

to the number of TBHP molecules in the complex). The LUMO + 5 of the complexes was the lowest unoccupied orbital which had significant contribution at TBHP (the orbital energies of HOMO − 10 to LUMO + 9 of TTMST and the complexes as well as the LUMO − LUMO + 5 features of TTMST and the TTMST−TBHP complex are described in the Supporting Information, Table 1(S) and Figure 5(S)). The interaction between the LUMO of TBHP and the LUMO + 5 of TTMST results in a stabilized orbital and destabilized one(s). For TBHP hydrogen-bonded to TTMST, the σ^*(O−O) orbital energy was more stable by 24.2 kJ/mol with respect to that of TBHP. When more TBHP molecules are hydrogen-bonded, the σ^*(O−O) orbital energy is even lower; with four TBHP molecules the stabilization is 31.9 kJ/mol. Therefore, we may infer that when more TBHP molecules are hydrogen-bonded, the complex is more active in epoxidation.

To clarify and understand the catalytic nature of the Ti in TTMST, the properties of the interaction of TBHP with TTMSS (tetrakis(trimethylsiloxy)silicon, $Si(OSiMe_3)_4$) were theoretically investigated at the B3PW91/6-311G(d) level of theory and compared with those of the TTMST−TBHP interaction. The geometry of TTMSS is similar to that of TTMST, although the Si(center)−O bond length is slightly shorter than the Ti−O bond length (Table 2). TTMSS also forms a hydrogen-bonding complex with TBHP with a larger binding energy (6.66 kJ/mol, BSSE corrected). The shorter hydrogen-bonding distance of TTMSS−TBHP supports the stronger interaction (Table 2). The Mulliken charges of oxygen atoms in TTMST and TTMSS are similar, and hence, the polarity of the bond does not explain the strength of the hydrogen bonds (Table 2).

Furthermore, Kohn−Sham orbitals of TTMSS and the TTMSS−TBHP complex were analyzed. The LUMO of TTMSS is the energetically most proximate orbital to the LUMO of TBHP (the orbital energies of HOMO − 10 to LUMO + 9 of TTMSS and the TTMSS−TBHP complex are shown in the Supporting Information, Table 1(S)). Similar to the case of TTMST−TBHP, the LUMO of TTMSS interacts with the LUMO of TBHP, which results in the stabilization of σ^*(O−O) of TBHP (Figure 11). There are two main differences when the TTMSS−TBHP orbitals are compared with the orbitals of the TTMST−TBHP complex. First, the σ^*(O−O) orbital stabilization is less due to the higher LUMO energy of TTMSS compared to the LUMO + 5 energy of TTMST (Figures 10 and 11). Second, the σ^*(O−O) orbital of the TTMSS−TBHP complex does not have a delocalized nature as in the TTMST−TBHP complex because of the localized character of the LUMO of TTMSS. The LUMO + 5 delocalized character of TTMST and the TTMST−TBHP complex are due to the d-orbitals of Ti, which are missing in TTMSS. These two differences, namely, orbital stabilization and delocalization, are probably crucial for the catalytic ability of TTMST. The stabilization of the σ^*(O−O) orbital is required for an epoxidation rate enhancement, and also the delocalized character of the σ^*(O−O) orbital may be important for activation of π(C═C) of olefins. When olefins interact with TBHP in the TTMST matrix, not necessarily in the proximity of TBHP, the delocalized orbital can interact with π(C═C), which leads to weakening of the O−O bond of TBHP and promotes epoxidation. In addition, the highly mobile nature of TBHP in the TTMST matrix as revealed by the spectroscopic experiments and the low binding

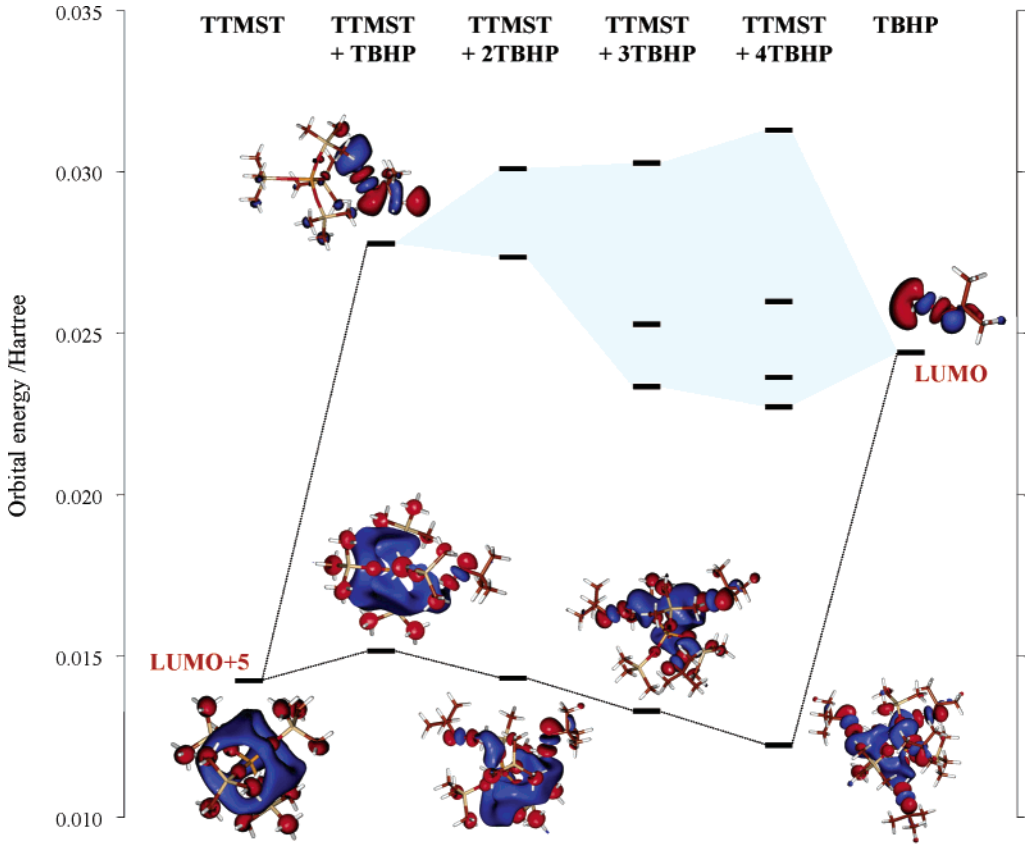

Figure 10. Orbital interaction and energy diagram between the LUMO + 5 of TTMST and the LUMO of TBHP.

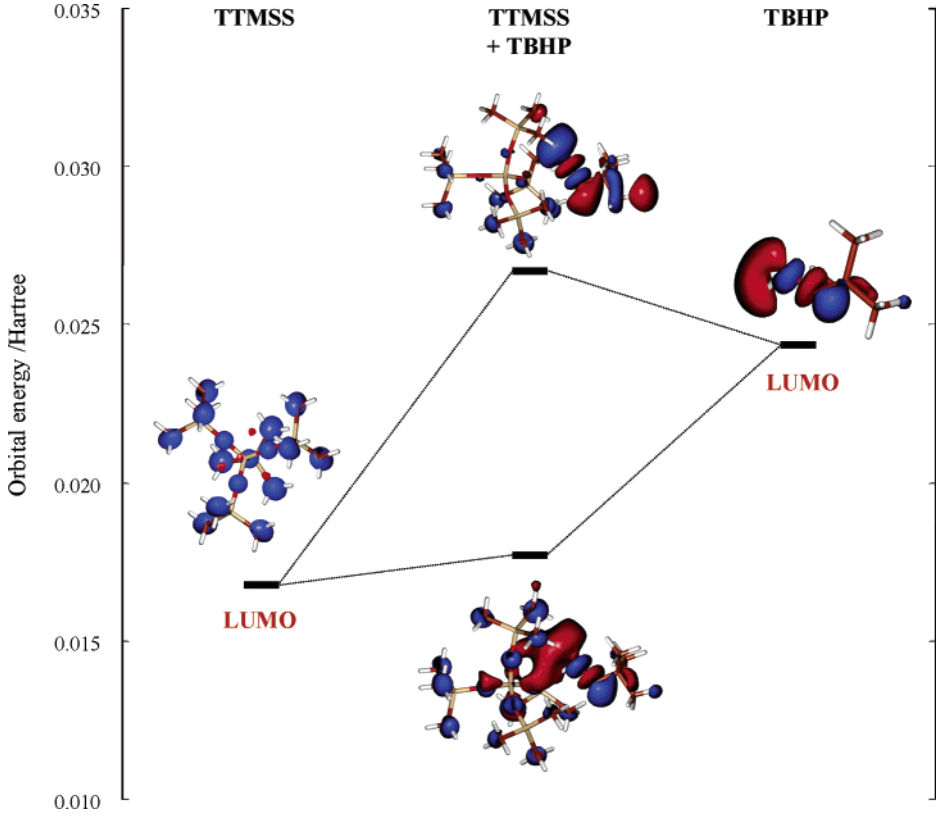

Figure 11. Orbital interaction and energy diagram between the LUMO of TTMSS and the LUMO of TBHP.

energy may assist and enhance collision of TBHP and olefins in the TTMST matrix.

The catalytic function of Ti is likely more due to the orbital interactions and the weak hydrogen-bonding than to the electrostatic effects. The stabilization and delocalization of TBHP σ^*(O−O) as well as the high mobility of TBHP in the hydrogen-bonded complexes could be the origin of the excellent catalytic performance of TTMST.

Epoxidation Mechanism and Comparison between the TS-1−H_2O_2 and TTMST−TBHP Systems. There are several differences between the two catalytic systems. A major difference is the effect of water presence on epoxidation activity. The TS-1−H_2O_2 catalysis occurs in aqueous medium, and also H_2O_2 can form water after oxygen transfer; hence, it is expected that water exists near the active center in the TS-1−H_2O_2 system. Recent experimental and theoretical studies on the TS-1−H_2O_2 system consider water to contribute to the active site formation,[17,45−47] promoting TiOOH (η^2) hydroperoxo complex formation in the Ti(−OSi)$_3$ moiety; although similar to the current study, H_2O_2 weakly interacting with the active Ti center is reported.[10] There are also some studies reporting TiOOR and TiOOSi to be the active species.[13,48] In the case of TTMST, water completely cleaves the Ti−O−Si bond irreversibly and deactivates the catalyst. In the TS-1−H_2O_2 system, water is always present but the catalyst is still active. This may be due to the rigid framework of TS-1, which allows condensation of OH groups formed by hydrolysis as observed by IR,[14] i.e., −Ti(OH) + (HO)Si− ⇄ −Ti−O−Si− + H_2O, while in the case of TTMST the hydrolyzed Me_3SiOH is far less likely present in the proximity of TiOH.

The current spectroscopic studies showed that the Ti−O−Si bond of TTMST is not cleaved upon TBHP addition and during epoxidation. This is an important fact that allows exclusion of "defect" models as proposed for the TS-1 system, i.e., a less than four −OSi− coordinated environment as the active center. Our computational investigations support that hydrogen-bonding of TBHP is the main interaction mode leading to the activation of the O−O bond. The differences mentioned above imply that the epoxidation mechanisms of the two systems have fewer common features than often advocated in the literature.

Conclusion

The combination of spectroscopic and computational studies allowed shedding light on the interactions between the reactants and the single-site homogeneous Ti−Si catalyst during epoxidation. The Ti−O−Si bond of TTMST is cleaved in the presence of water, while TBHP does not cleave this bond and forms weak hydrogen-bonded complexes, as supported by our IR, NMR, and computational investigations. The cleavage of the Ti−O−Si bond was also not observed during epoxidation. The hydrogen-bonding of TBHP to TTMST lowers the σ^*(O−O) orbital energy of TBHP, and thereby activates the O−O bond of TBHP for epoxidation. When all four Ti−O−Si bonds are hydrogen-bonded, the O−O bond becomes most active. CHol only weakly interacts with TTMST, but the interaction becomes stronger when CHol interacts with the TTMST−TBHP complex. The σ^*(O−O) orbital energy stabilization and delocalization as well as the highly mobile TBHP in the TTMST matrix seem to play key roles in epoxidation. The study, using an active model homogeneous catalyst, may provoke another view on the epoxidation mechanisms governing heterogeneous Ti−Si-based catalysts.

Acknowledgment. We thank CSCS, Manno, Switzerland, and ETH-Zürich for computational time. Financial support by the Foundation Claude and Giuliana is kindly acknowledged.

Supporting Information Available: Equilibrium geometry of TBHP, conformation analysis of CHol IR study of OH stretching region of TTMST-TBHP, TTMST-CHol interaction study, and orbital analysis. This material is available free of charge via the Internet at http://pubs.acs.org.

Note Added after ASAP Posting. This article was released ASAP on 7/7/2004. Table 2 has been revised. The correct version was posted on 7/19/2004.

References and Notes

(1) Jørgensen, K. A. *Chem. Rev.* **1989**, *89*, 431−458.
(2) Dusi, M.; Mallat, T.; Baiker, A. *Catal. Rev.−Sci. Eng.* **2000**, *42*, 213−278.
(3) Gao, Y.; Hanson, R. M.; Klunder, J. M.; Ko, S. Y.; Masamune, H.; Sharpless, K. B. *J. Am. Chem. Soc.* **1987**, *109*, 5765−5780.
(4) Woodard, S. S.; Finn, M. G.; Sharpless, K. B. *J. Am. Chem. Soc.* **1991**, *113*, 106−113.
(5) Finn, M. G.; Sharpless, K. B. *J. Am. Chem. Soc.* **1991**, *113*, 113−126.
(6) Wu, Y. D.; Lai, D. K. W. *J. Am. Chem. Soc.* **1995**, *117*, 11327−11336.
(7) Notari, B. *Catal. Today* **1993**, *18*, 163−172.
(8) Lane, B. S.; Burgess, K. *Chem. Rev.* **2003**, *103*, 2457−2473.
(9) Tozzola, G.; Mantegazza, M. A.; Ranghino, G.; Petrini, G.; Bordiga, S.; Ricchiardi, G.; Lamberti, C.; Zulian, R.; Zecchina, A. *J. Catal.* **1998**, *179*, 64−71.
(10) Vayssilov, G. N.; van Santen, R. A. *J. Catal.* **1998**, *175*, 170−174.
(11) Gleeson, D.; Sankar, G.; Catlow, C. R. A.; Thomas, J. M.; Spano, G.; Bordiga, S.; Zecchina, A.; Lamberti, C. *Phys. Chem. Chem. Phys.* **2000**, *2*, 4812−4817.
(12) Ricchiardi, G.; Damin, A.; Bordiga, S.; Lamberti, C.; Spano, G.; Rivetti, F.; Zecchina, A. *J. Am. Chem. Soc.* **2001**, *123*, 11409−11419.
(13) Munakata, H.; Oumi, Y.; Miyamoto, A. *J. Phys. Chem. B* **2001**, *105*, 3493−3501.
(14) Lin, W. Y.; Frei, H. *J. Am. Chem. Soc.* **2002**, *124*, 9292−9298.
(15) Damin, A.; Bonino, F.; Ricchiardi, G.; Bordiga, S.; Zecchina, A.; Lamberti, C. *J. Phys. Chem. B* **2002**, *106*, 7524−7526.
(16) Damin, A.; Bordiga, S.; Zecchina, A.; Lamberti, C. *J. Chem. Phys.* **2002**, *117*, 226−237.
(17) Wells, D. H.; Delgass, W. N.; Thomson, K. T. *J. Am. Chem. Soc.* **2004**, *126*, 2956−2962.
(18) Crocker, M.; Herold, R. H. M.; Orpen, A. G. *Chem. Commun.* **1997**, 2411−2412.
(19) Crocker, M.; Herold, R. H. M.; Orpen, A. G.; Overgaag, M. T. A. *J. Chem. Soc., Dalton Trans.* **1999**, 3791−3804.
(20) Maschmeyer, T.; Klunduk, M. C.; Martin, C. M.; Shephard, D. S.; Thomas, J. M.; Johnson, B. F. G. *Chem. Commun.* **1997**, 1847−1848.
(21) Abbenhuis, H. C. L.; Krijnen, S.; van Santen, R. A. *Chem. Commun.* **1997**, 331−332.
(22) Voigt, A.; Murugavel, R.; Montero, M. L.; Wessel, H.; Liu, F. Q.; Roesky, H. W.; Uson, I.; Albers, T.; Parisini, E. *Angew. Chem., Int. Ed. Engl.* **1997**, *36*, 1001−1003.
(23) Skowronska-Ptasinska, M. D.; Vorstenbosch, M. L. W.; van Santen, R. A.; Abbenhuis, H. C. L. *Angew. Chem., Int. Ed.* **2002**, *41*, 637−639.
(24) Gesser, H. D.; Goswami, P. C. *Chem. Rev.* **1989**, *89*, 765−788.
(25) Hutter, R.; Mallat, T.; Baiker, A. *J. Catal.* **1995**, *153*, 177−189.
(26) Holland, M. A.; Pickup, D. M.; Mountjoy, G.; Tsang, E. S. C.; Wallidge, G. W.; Newport, R. J.; Smith, M. E. *J. Mater. Chem.* **2000**, *10*, 2495−2501.
(27) Deng, Y.; Maier, M. F. *J. Catal.* **2001**, *199*, 115−122.
(28) Beck, C.; Mallat, T.; Bürgi, T.; Baiker, A. *J. Catal.* **2001**, *204*, 428−439.
(29) Beck, C.; Mallat, T.; Baiker, A. *New J. Chem.* **2003**, *27*, 1284−1289.
(30) Johnson, B. F. G.; Klunduk, M. C.; Martin, C. M.; Sankar, G.; Teate, S. J.; Thomas, J. M. *J. Organomet. Chem.* **2000**, *596*, 221−225.
(31) Tyrrell, H. J. W.; Harris, K. R. *Diffusion in Liquids*; Butterworths: London, 1984.
(32) Frisch, M. J.; Trucks, G. W.; Schlegel, H. B.; Scuseria, G. E.; Robb, M. A.; Cheeseman, J. R.; Zakrzewski, V. G.; Montgomery, J. A., Jr.; Stratmann, R. E.; Burant, J. C.; Dapprich, S.; Millam, J. M.; Daniels, A. D.; Kudin, K. N.; Strain, M. C.; Farkas, O.; Tomasi, J.; Barone, V.; Cossi, M.; Cammi, R.; Mennucci, B.; Pomelli, C.; Adamo, C.; Clifford, S.; Ochterski, J.; Petersson, G. A.; Ayala, P. Y.; Cui, Q.; Morokuma, K.; Malick, D. K.; Rabuck, A. D.; Raghavachari, K.; Foresman, J. B.; Cioslowski, J.; Ortiz, J. V.; Stefanov, B. B.; Liu, G.; Liashenko, A.; Piskorz, P.; Komaromi, I.; Gomperts, R.; Martin, R. L.; Fox, D. J.; Keith, T.; Al-Laham, M. A.; Peng, C. Y.; Nanayakkara, A.; Gonzalez, C.; Challacombe, M.; Gill, P. M. W.; Johnson, B. G.; Chen, W.; Wong, M. W.; Andres, J. L.; Head-Gordon, M.; Replogle, E. S.; Pople, J. A. *Gaussian 98*, revision A.7; Gaussian, Inc.: Pittsburgh, PA, 1998.
(33) Frisch, M. J.; Trucks, G. W.; Schlegel, H. B.; Scuseria, G. E.; Robb, M. A.; Cheeseman, J. R.; Montgomery, J. A., Jr.; Vreven, T.; Kudin, K. N.; Burant, J. C.; Millam, J. M.; Iyengar, S. S.; Tomasi, J.; Barone, V.; Mennucci, B.; Cossi, M.; Scalmani, G.; Rega, N.; Petersson, G. A.;

Nakatsuji, H.; Hada, M.; Ehara, M.; Toyota, K.; Fukuda, R.; Hasegawa, J.; Ishida, M.; Nakajima, T.; Honda, Y.; Kitao, O.; Nakai, H.; Klene, M.; Li, X.; Knox, J. E.; Hratchian, H. P.; Cross, J. B.; Adamo, C.; Jaramillo, J.; Gomperts, R.; Stratmann, R. E.; Yazyev, O.; Austin, A. J.; Cammi, R.; Pomelli, C.; Ochterski, J. W.; Ayala, P. Y.; Morokuma, K.; Voth, G. A.; Salvador, P.; Dannenberg, J. J.; Zakrzewski, V. G.; Dapprich, S.; Daniels, A. D.; Strain, M. C.; Farkas, O.; Malick, D. K.; Rabuck, A. D.; Raghavachari, K.; Foresman, J. B.; Ortiz, J. V.; Cui, Q.; Baboul, A. G.; Clifford, S.; Cioslowski, J.; Stefanov, B. B.; Liu, G.; Liashenko, A.; Piskorz, P.; Komaromi, I.; Martin, R. L.; Fox, D. J.; Keith, T.; Al-Laham, M. A.; Peng, C. Y.; Nanayakkara, A.; Challacombe, M.; Gill, P. M. W.; Johnson, B.; Chen, W.; Wong, M. W.; Gonzalez, C.; Pople, J. A. *Gaussian 03*, revision B.03; Gaussian, Inc.: Pittsburgh, PA, 2003.

(34) Becke, A. D. *J. Chem. Phys.* **1993**, *98*, 5648−5652.

(35) Perdew, J. P.; Wang, Y. *Phys. Rev. B* **1992**, *45*, 13244−13249.

(36) Wachters, A. J. *J. Chem. Phys.* **1970**, *52*, 1033−&.

(37) Hay, P. J. *J. Chem. Phys.* **1977**, *66*, 4377−4384.

(38) Raghavachari, K.; Trucks, G. W. *J. Chem. Phys.* **1989**, *91*, 1062−1065.

(39) Boys, S. F.; Bernardi, F. *Mol. Phys.* **1970**, *19*, 553−&.

(40) Einstein, A. *Investigation on the theory of the brownian movement*; Dover Publications, Inc.: New York, 1956.

(41) Deubel, D. V. *J. Org. Chem.* **2001**, *66*, 3790−3796.

(42) Kühn, F. E.; Santos, A. M.; Roesky, P. W.; Herdtweck, E.; Scherer, W.; Gisdakis, P.; Yudanov, I. V.; Di Valentin, C.; Rösch, N. *Chem.—Eur. J.* **1999**, *5*, 3603−3615.

(43) Yudanov, I. V.; Gisdakis, P.; Di Valentin, C.; Rösch, N. *Eur. J. Inorg. Chem.* **1999**, 2135−2145.

(44) Di Valentin, C.; Gisdakis, P.; Yudanov, I. V.; Rösch, N. *J. Org. Chem.* **2000**, *65*, 2996−3004.

(45) Zicovich-Wilson, C. M.; Dovesi, R.; Corma, A. *J. Phys. Chem. B* **1999**, *103*, 988−994.

(46) Sinclair, P. E.; Sankar, G.; Catlow, C. R. A.; Thomas, J. M.; Maschmeyer, T. *J. Phys. Chem. B* **1997**, *101*, 4232−4237.

(47) Sankar, G.; Thomas, J. M.; Catlow, C. R. A.; Barker, C. M.; Gleeson, D.; Kaltsoyannis, N. *J. Phys. Chem. B* **2001**, *105*, 9028−9030.

(48) Fujiwara, M.; Wessel, H.; Hyung-Suh, P.; Roesky, H. W. *Tetrahedron* **2002**, *58*, 239−243.

(49) Assael, M. J.; Dalaouti, N. K.; Dymond, J. H. *Int. J. Thermophys.* **2000**, *21*, 291−299.